

DESIGN AND DEVELOPMENT OF AN AGILE, MAN PORTABLE UNMANNED GROUND VEHICLE

Karl Iagnemma, Martin Udengaard, Genya Ishigami
Massachusetts Institute of Technology, Department of Mechanical Engineering
Cambridge, MA 02139

Matthew Spenko*, Sinan Oncu, Imad Khan
Illinois Institute of Technology, Mechanical, Materials, and Aerospace Department
Chicago, IL 60616

James Overholt, Gregory Hudas
U.S. Army Tank Automotive Research Development and Engineering Center (TARDEC)
Detroit Arsenal, Warren, MI 48089

ABSTRACT

An omnidirectional unmanned ground vehicle (UGV) is able to move in any planar direction regardless of its current pose. To date, nearly all designs and analyses of omnidirectional robots have considered the case of motion on flat, smooth terrain. This paper presents the design, analysis, and prototype development of a man portable omnidirectional UGV designed for operation in rough terrain. Design guidelines are presented that are derived from geometric constraints on wheel and linkage sizes. The effects of terrain roughness and loss of wheel contact on UGV mobility are also analyzed. A framework for UGV design optimization is presented that considers vehicle kinematic isotropy, wheel-terrain interaction properties, predicted obstacle traversability, and maximum traversable distance over various outdoor terrain types. The results are used to design two small (i.e. 1m characteristic length), lightweight (i.e. approximately 25 kg) UGV prototypes.

1. INTRODUCTION

The US Army has steadily been increasing its use of unmanned ground vehicles in an effort to remove soldiers from dangerous situations. UGVs can be employed in various scenarios, including inspection and disposal of improvised explosive devices and mule applications. To maximize their effectiveness in these situations, UGVs must navigate cluttered environments in the presence of obstacles, ideally at high speeds. This requires that UGVs be highly agile (i.e. capable of rapidly changing directions without a significant decrease in speed) even in rough, outdoor terrain. Currently, the majority of UGVs under development are either tracked or Ackermann-steered vehicles, neither of which generally exhibit high agility. Ideally, UGVs would exhibit omnidirectional mobility, i.e. the ability to move (kinematically) in any planar direction regardless of current pose. The research

described here targets two key Army need areas: (1) high-speed, effective operations in off-road and cluttered urban environments, and (2) platform mobility capabilities improvement.

To date, nearly all omnidirectional vehicle designs have been intended for use on flat, clean, indoor surfaces. These omnidirectional vehicles rely on friction drives or specialized wheels (e.g. the Mecanum wheel [2]) that are not suitable for outdoor environments because their slender rollers can easily become clogged with dirt and debris. This paper presents an omnidirectional vehicle design that is specifically intended for outdoor use. This design utilizes active split offset caster (ASOC) drive modules (see Fig. 1) [8]. ASOC modules utilize conventional wheels and can easily be coupled with classical suspension elements, which makes them suitable for use in rough, outdoor environments [3]. They can also be designed to accommodate a large variation in wheel diameter and width, which allows them to tolerate large loads while maintaining low ground pressure.

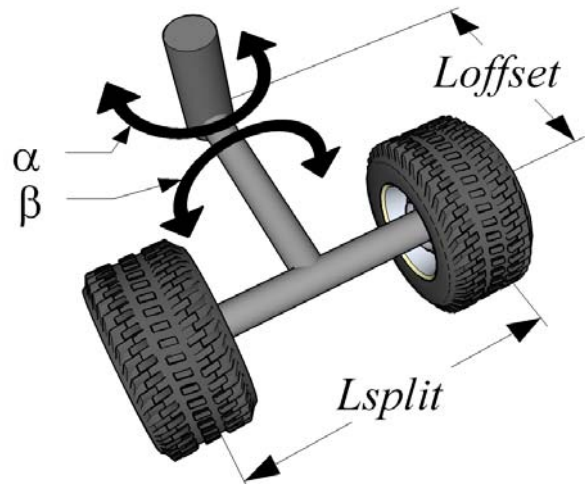


Fig. 1: Example of an active split offset caster drive module.

In this paper, design considerations, both theoretical and practical, for an ASOC-driven omnidirectional UGV for operation in rough terrain are presented. The design parameters examined include the number of ASOC modules, ASOC kinematic parameters, module location, and wheel geometry. The parameters are optimized for kinematic isotropy, ability to maintain ground contact, obstacle height, and maximum traversable distance over four diverse terrain types. The results of this optimization are used to design two small (i.e. 1 m characteristic length), lightweight (i.e. approximately 25 kg) UGV prototypes. A CAD model of one of the prototypes is shown in Figure 2. Two models have been designed and fabricated to experimentally study the effects of different suspension configurations on the above-mentioned parameters.

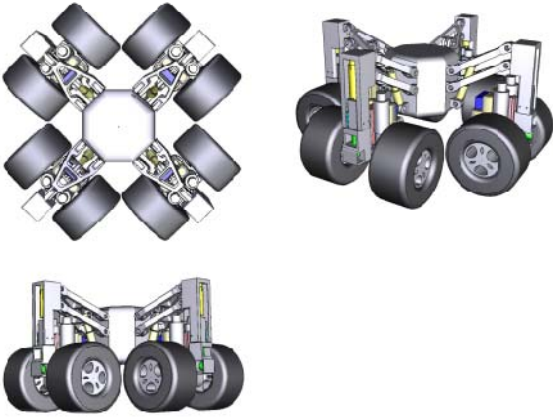


Fig. 2: CAD Model of agile, man portable UGV

2. ACTIVE SPLIT OFFSET CASTER DESCRIPTION

ASOC drive modules possess the ability to achieve omnidirectional motion via a driven wheel pair. Fig. 1 shows the ASOC module geometry considered in this study. The assembly consists of a split wheel pair, a connecting axle, and an offset link connecting the wheel pair to the UGV body. Each wheel is independently driven. The wheel pair/axle assembly rotates passively about axis α . This axis connects the ASOC module to a robot body or a passive or active suspension element. L_{offset} is the distance between the axis α and the wheel axes. L_{split} is the distance between the wheels. Angle β is used as rotational degree of freedom in one of the suspension designs presented in this paper.

By independently controlling each wheel's velocity, an ASOC module can produce arbitrary (planar) translational velocities at a point along its α axis. Two or more ASOC modules attached to a rigid robot body can thus produce arbitrary translational and rotational robot velocities. Therefore, an ASOC-driven omnidirectional robot must minimally employ two ASOC modules, and can employ more to meet other design requirements

related to thrust, ground pressure, tip-over stability, etc. Note that passive or active casters can also be used to augment ASOC modules to meet these requirements. A kinematic analysis of ASOC modules is presented in [3].

3. DESIGN OBJECTIVES

The design considered in this paper is a man-portable, battery powered UGV with a maximum enclosed envelope of one cubic meter and maximum mass of approximately 25 kg with an additional payload of 40 kg. The primary design objective is to maximize traversable distance over a range of outdoor terrain types while maintaining a high level of mobility (quantified by system kinematic isotropy, the ability of an ASOC module to maintain ground contact, and traversable obstacle height). The robot must operate under its own power, and therefore should maximize mass efficiency to increase its battery payload. It should also minimize power loss from motion resistance in deformable terrain. Factors influencing the design space include wheel width, wheel radius, ASOC split and offset lengths, and the number and relative location of ASOC modules. Geometric constraints that bound the allowable design space must also be considered.

The CAD model shown in Fig. 2 uses four ASOC modules. This is a representative configuration that will be considered in this work; however the analysis is general and applies to robots with any number of ASOC modules.

4. GEOMETRIC CONSTRAINTS

The unique geometry of the ASOC and the large range of motion of each module constrain the size of some components. Potentially, a control algorithm could utilize the robot's redundancy to relax these constraints (by ensuring that wheel pairs are never directly oriented towards each other, for example). However, such an algorithm would likely reduce overall system mobility. Here, a geometric analysis of the ASOC module workspace and maximum pivot angle range of motion is presented.

The maximum allowable wheel size that does not risk ASOC interference can be calculated by simple geometric analysis of the module workspace. As seen in Fig. 3, the minimum distance between adjacent ASOC axes, d_a , must be at least twice the maximum radius of the ASOC workspace, $r_{workspace}$. This radius is the distance from the vertical axis to the most distal point on the wheel:

$$r_{workspace} = \sqrt{(L_{offset} + r_{wheel})^2 + (0.5L_{split} + w_{wheel})^2} \quad (1)$$

where r_{wheel} and w_{wheel} are the wheel radius and width.

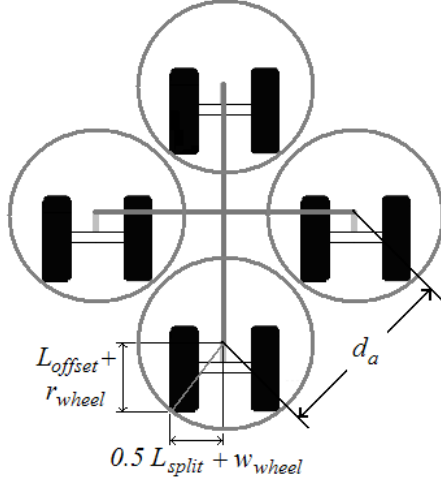


Fig. 3: The circles represent the boundaries of the ASOC module workspace.

Additional geometric constraints can exist based on the type of suspension employed. For example, if angle β as shown in Fig. 1 can freely rotate, then further analysis is warranted [5].

5. ISOTROPY ANALYSIS

All omnidirectional mobile robots are kinematically able to instantaneously travel in any planar direction. However, some omnidirectional mobile robots exhibit preferred directions of travel, while others exhibit equal mobility in all directions. Hence, isotropy is used to quantify the system's omnidirectional mobility.

Kinematic isotropy is defined as the condition in which a robot possesses a constant input/output velocity ratio for all possible output velocity directions [4]. An isotropy metric measures how near a robot is to the isotropy condition, and increases from 0.0 for a singular configuration (i.e. non-omnidirectional) to 1.0 for kinematic isotropy. Ideally, an omnidirectional robot should possess a metric value of 1.0 for all joint space configurations, and thus not have a preferred direction of travel. This simplifies path planning and navigation by eliminating the effect of robot orientation on movement capability. The output directions considered in this study are two planar translations in the robot body frame, and rotation about the robot body frame vertical axis.

The isotropy metric for a given robot configuration can be computed as the ratio of the smallest to largest eigenvalues of the Jacobian matrix relating the driving module velocities to the robot body velocities [4]. The isotropy metric can be averaged over the entire configuration space (in this case, the rotation angles between each ASOC and the body, α) to yield an average measure of performance that could be used to compare candidate omnidirectional mobile robot designs.

5.1 Effect of ASOC Kinematic Parameters on Isotropy

Fig. 4 illustrates the effects of ASOC module kinematic parameters on isotropy, where L_{offset} and L_{split} were varied over values that represent a practical design space. Note that in Fig. 4, L_{offset} and L_{split} are normalized by the length of the longest side of the robot body.

An iso-height exists at an isotropy value of 1.0. This iso-height occurs at $L_{split}/L_{offset} = 2.0$. The sensitivity of isotropy to perturbations in L_{split} and L_{offset} is relatively high; a 10% change in L_{split} or L_{offset} decreases the isotropy metric value by up to 45% for small ASOC module sizes.

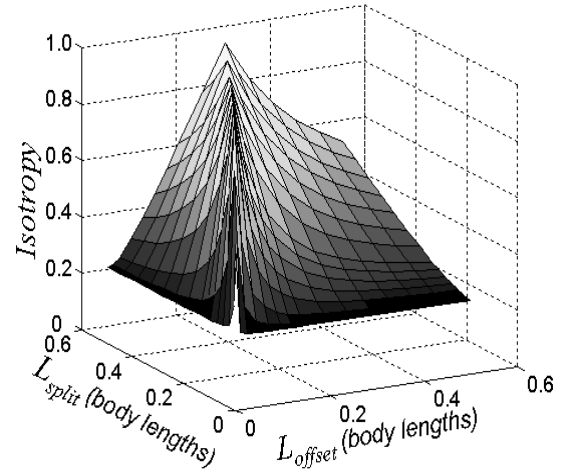


Fig. 4: Average isotropy for a four ASOC UGV.

Fig. 5 is a plot of isotropy values over a range of L_{split} / L_{offset} ratios. From this figure it can be seen that there exists a single isotropy value for each L_{split} / L_{offset} ratio, indicating that isotropy is not an independent function of both L_{split} and L_{offset} . This is a useful insight for omnidirectional robot design. This also explains the sensitivity of isotropy to changes in L_{split} and L_{offset} for small ASOC modules sizes, since a unit change in L_{split} or L_{offset} results in a relatively large change in L_{split} / L_{offset} for small parameter values.

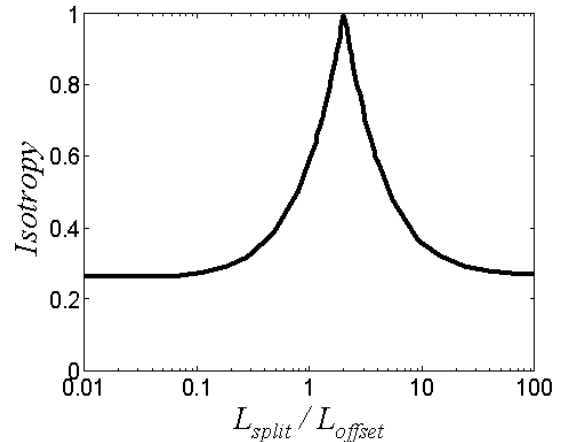


Fig. 5: Average isotropy for a robot driven by four ASOC modules as a function of L_{split} / L_{offset} .

5.2 Effect of ASOC Module Location on Isotropy

The relative location of ASOC modules also affects isotropy. A plot of isotropy as a function of relative ASOC angular location is presented in Fig. 6. Note that a robot with three modules, shown in Fig. 7, was chosen for analysis so that the results can be visually presented in two dimensions. Each ASOC had an L_{split} / L_{offset} ratio of 2.0. ASOC interference was neglected.

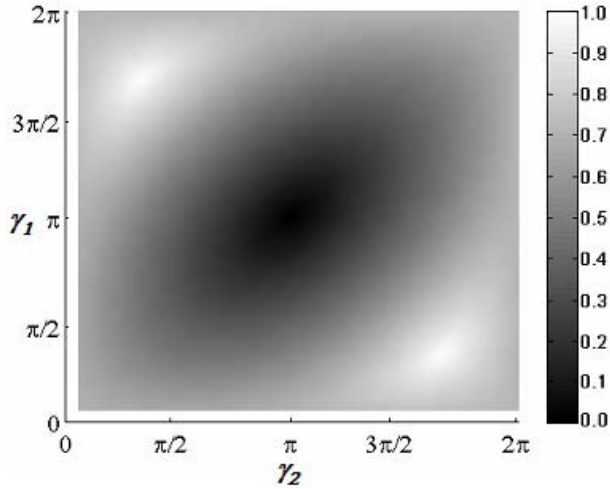


Fig. 6: Isotropy as a function of ASOC module relative location

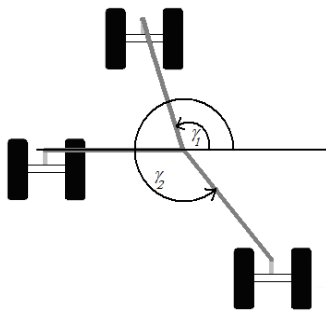


Fig. 7: Top view of representative robot for ASOC location analysis

To maximize isotropy, it can be shown that the ASOC modules should be equally spaced to obtain the maximum isotropy values (1.0). The value drops to 0.0 for the degenerate case where all ASOC modules coincide. A similar phenomenon is observed for robots with any number of ASOC modules.

5.3 Effect of Loss of Wheel Contact on Isotropy

When traversing rough terrain, loss of contact may occur between the wheels and the ground. In this case, system mobility will be decreased. An analysis of the isotropy of robots without full ground contact is presented in Table 1. For comparison, robots with two, three, and four ASOC modules are examined. Each ASOC is allowed to possess full, partial (one wheel on the ground), or no ground contact.

Table 1: Effect of Loss of Wheel Contact on Isotropy.

# ASOC	# no contact ASOC	# partial contact ASOCs				
		0	1	2	3	4
2	0	1.000	0.464	0.000	N/A	N/A
3	0	1.000	0.706	0.504	0.270	N/A
	1	0.577	0.367	0.000	N/A	N/A
4	0	1.000	0.791	0.656	0.544	0.399
	1	0.707	0.574	0.482	0.259	N/A
	2	0.414	0.265	0.000	N/A	N/A

As expected, loss of wheel contact causes reduced isotropy due to a loss of full controllability of the ASOC modules. It can be observed that a four ASOC robot with one module that has completely lost terrain contact does not perform as well as a three ASOC robot in full contact. This is due to the fact that a robot with three ASOCs has evenly spaced modules. Also, given an identical number of wheels without terrain contact (e.g., 0 no contact and 2 partial contact vs. 1 no contact and 0 partial contact), a robot generally has higher isotropy when terrain contact is lost on the same ASOC, since more modules remain fully engaged with the ground. The isotropy loss from partial contact ASOC modules reinforces the importance of the axle pivot.

Finally, a robot with a greater number of ASOCs will have a relatively smaller drop in isotropy for each lost wheel contact, but may have increased difficulty keeping all wheels in contact with the ground due to increased suspension complexity. Additional modules also add mass while decreasing the allowable wheel size and available battery mass.

5.4 Effect of Terrain Roughness on Isotropy

UGV isotropy can also be affected by terrain roughness. Variation in terrain inclination among ASOC modules, or among ASOC module wheel pairs, can cause a change in the effective value of L_{split} with respect to the body frame, which yields a change in L_{split} / L_{offset} and thus a change in isotropy. Fig. 8 illustrates how L_{split} is reduced if the angle, β , is allowed to freely rotate.

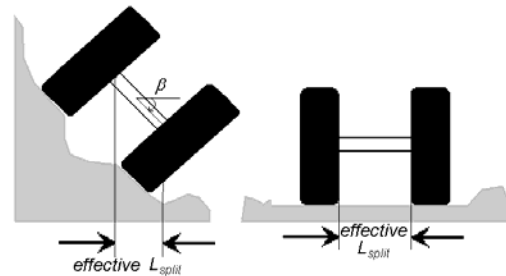


Fig. 8: ASOC module on flat and rough terrain.

Alternatively, if the angle β is kept fixed, L_{split} can be kept constant; however, depending on the design of the

suspension elements, L_{offset} may change as a function of the suspension travel. For example, Fig. 9 illustrates a four-bar linkage suspension system in which L_{offset} varies as a function of suspension travel.

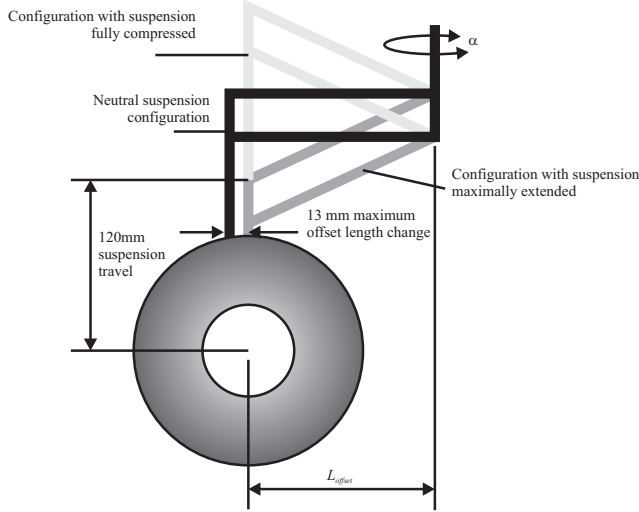


Fig. 9: A four-bar linkage design’s kinematic isotropy is independent of terrain inclination, but changes as a function of obstacle height.

In Fig. 10, a contour plot is presented of the average isotropy over a range of static robot configurations and terrain angles. It can be seen that the L_{split} / L_{offset} ratio with the largest isotropy value increases with the maximum terrain angle. Larger angles decrease the effective ratio and thus the “true” ratio must therefore increase. Maximum average isotropy also decreases slightly with increasing terrain angle. Table 2 summarizes these findings.

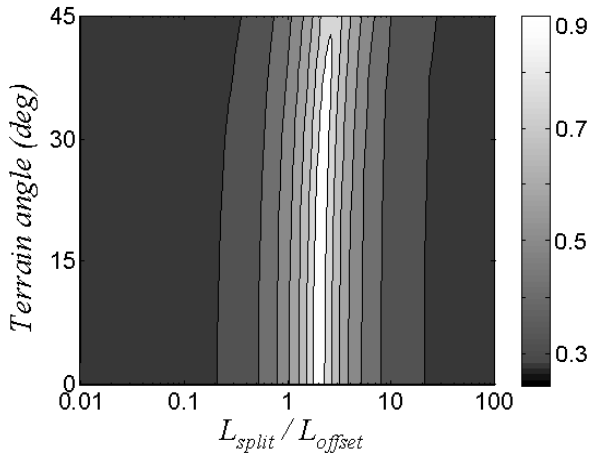


Fig. 10: Average isotropy as a function of L_{split} / L_{offset} and terrain angle.

Table 2: Effect of Terrain on Isotropy and Ideal Split/Offset Ratio

Terrain angle	Max isotropy	Optimum
		L_{split} / L_{offset} ratio
0° (flat)	1.000	2.00
0-15o	0.987	2.05
0-30o	0.950	2.27
0-45o	0.895	2.70

6. DESIGN OPTIMIZATION

A design optimization was performed using the objectives outlined in Section III and constraints outlined in Section IV. The optimization varies the number of ASOC modules, L_{split} , L_{offset} , r_{wheel} , and w_{wheel} . The objective function, J , is the sum of the normalized mobility parameters:

$$J = \frac{K}{K^*} + \frac{\beta_{max}}{\beta_{max}^*} + \frac{h}{h^*} + \frac{d_{max}}{d_{max}^*}, \quad (3)$$

where K is the kinematic isotropy, β_{max} is the maximum β axis pivot, h is the maximum traversable obstacle height, and d_{max} is the maximum traversable distance. The star superscript refers to the maximum value of each parameter in the design space. The optimization consisted of a full factorial analysis over the design space to maximize the value of the objective function.

In this analysis, maximum pivot angle and kinematic isotropy are calculated as described in Sections 4 and 5. The maximum traversable obstacle height is assumed to be a linear function of the wheel radius.

The optimization algorithm estimates maximum traversable distance by first determining the maximum available onboard energy. For the purposes of this study, it is assumed that the robot is powered by batteries with an energy density ρ_{energy} of 576 kJ/kg (similar to that of lithium-ion batteries). The maximum allowable onboard battery mass, $M_{battery}$, is the difference between the non-battery mass (i.e., wheels, structural components, electronics, etc.) and the predetermined total allowable mass. In this study, the total available mass limit was 65 kg which we set as an upper bound considering the robots payload. Wheel and ASOC masses are computed as a function of their sizes.

The energy consumed during forward travel is then estimated using Bekker’s formulation for compaction resistance [5].

$$CR = \frac{n_{wheels}}{(3-n) \binom{2n+2}{2n+1} (n+1) w_{wheel} \binom{1}{2n+1} \left(k_c / w_{wheel} + k_\phi \right) \binom{1}{2n+1}} \left[\frac{3 Mg}{\sqrt{r_{wheel}}} \right]^{\binom{2n+2}{2n+1}} \quad (4)$$

In the equation above, CR is the compaction resistance (N), M is the total robot mass (kg), g is gravity, n_{wheels} is the number of wheels, and n , k_c , and k_ϕ are terrain physical constants (shown in Table 3 [6, 7]). Note that this estimate is for straight driving and does not take into account other resistive forces (such as bulldozing forces) or energy used by other onboard devices.

Table 3: Terrain Parameters

Terrain type	n	k_c (kPa/m ⁿ⁻¹)	k_ϕ (kPa/m ⁿ)
Dry sand	1.1	0.9	1523.4
Sandy loam	0.7	5.3	1515.0
Clayey soil	0.5	13.2	692.2
Snow	1.6	4.4	196.7

The maximum traversable distance is approximated as $d_{max} = M_{battery} \rho_{energy} / CR$. Since the optimization compares similar systems, motor and drivetrain efficiencies are assumed identical for all candidate designs and therefore are not considered in the calculations.

7. DESIGN OPTIMIZATION RESULTS

Table 4 compares the mobility parameters of UGVs with three, four, and five ASOC modules. The robots were optimized for travel over sandy loam. Results are presented relative to the robot with three ASOC modules. It can be observed that all four mobility parameters decreased as the number of ASOC modules increases.

Table 4: Effect of the Number of ASOCs on Mobility Parameters

# ASOCs	K	β_{max}	h	d_{max}
3	0%	0%	0%	0%
4	-0.4%	-1.3%	-6.1%	-38.8%
5	-2.2%	-16.2%	-60.9%	-54.7%

The robot with four ASOC modules has similar values of K , β_{max} , and h as the three ASOC robot, however, adding the fourth module decreases available battery mass, and therefore decreases d_{max} . The fifth ASOC module creates a smaller $r_{workspace}$ and hence a smaller L_{split} and r_{wheel} , resulting in lower β_{max} and h .

Table 5 shows the values of the geometric parameters for a three ASOC robot derived using the optimization algorithm and geometric constraints described above. Optimizations were calculated over the four terrain types shown in Table 3, assuming randomized rough terrain with an angle range of 0-30°. Table 6 shows the change in mobility parameter values for optimized designs compared to a baseline design with parameters

determined by engineering judgment ($L_{offset}=0.15$ m, $L_{split}=0.20$ m, $r_{wheel}=0.15$ m, $w_{wheel}=0.03$ m).

Table 5: Geometric Parameters from Optimization

Terrain type	L_{offset} (m)	L_{split} (m)	r_{wheel} (m)	w_{wheel} (m)
Dry sand	0.191	0.439	0.193	0.086
Sandy loam	0.144	0.325	0.148	0.167
Clayey soil	0.144	0.325	0.148	0.176
Snow	0.229	0.515	0.229	0.029

Table 6: Mobility Parameter Increases from Optimization

Terrain type	K	β_{max}	H	d_{max}
Dry sand	12.1%	98.1%	28.6%	23.5%
Sandy loam	13.2%	85.2%	-1.4%	46.6%
Clayey soil	13.2%	85.2%	-1.4%	45.0%
Snow	12.4%	115.3%	52.6%	26.6%

Note that the geometric parameter sets for relatively rigid terrains (i.e. sandy loam and clayey soil) had similar values. This implies that the robot could be adjusted to go from one surface to another by installing tires with a different width and changing the battery mass.

In all cases, the offset lengths were slightly smaller than the wheel radii, which yielded large allowable β tilt angles. The split offset ratios were all near 2.27:1, maximizing isotropy for the given terrain roughness range.

As presented, the optimizations for the relatively deformable terrains (i.e. dry sand and snow) resulted in wheels with larger radii, but narrower widths compared to those optimized for relatively rigid terrains. The large radii lead to decreased ground pressure and compaction resistance, while the thinner widths lead to decreased wheel weight. One could also minimize ground pressure by choosing a wider wheel, but for a given a depth of sinkage, a tall, narrow wheel has significantly less compaction resistance than a short, wide one. For the relatively rigid terrains, a wider wheel was preferred as it allowed a greater amount of onboard battery mass, thus increasing maximum traversable distance.

8. PROTOTYPE VEHICLE DESIGN

The results of the study were used to create two different prototype ASOC module designs for experimental validation. In addition to the results of the study, several practical design guidelines were considered. Effort was taken to minimize the rotational moment of inertia about the α degree of freedom and minimize the ratio of unsprung to sprung mass.

The two designs that were chosen are shown in Fig. 11 and Fig. 12. The design shown in Fig. 11 employs a four-bar linkage that ensures that L_{split} is constant and independent of terrain inclination. However, L_{offset} varies by as much as 13.4 mm such that the L_{split}/L_{offset} ratio can vary from 2 to 2.21 depending on the suspension compression/extension. The design also minimizes the upsprung/sprung mass ratio since the batteries are located on the sprung mass.

The design shown in Fig. 12 employs a passive degree of freedom about the β axis and an additional suspension element located between the ASOC and the central body. The resulting design should yield better conformity to inclined terrain at the expense of a worse unsprung/sprung mass ratio.

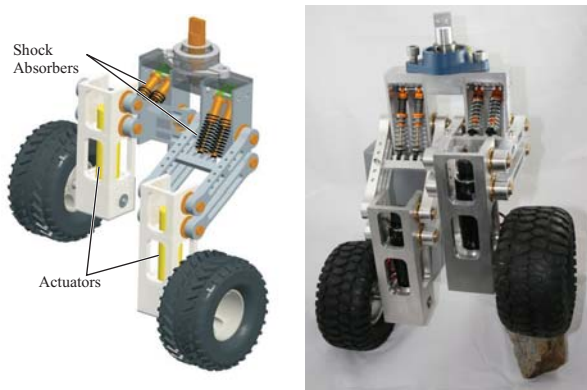


Fig. 11: Four-bar linkage suspension design.

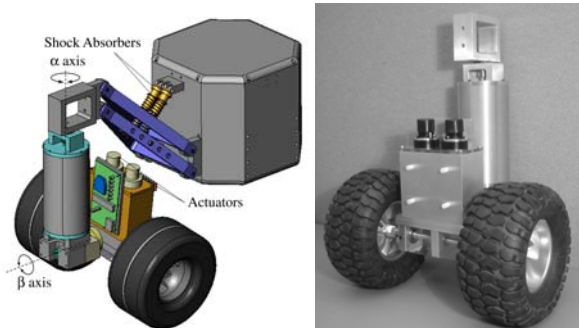


Fig. 12: β -axis pivot ASOC design.

The two designs have similar planar kinematic properties (wheel width, wheel radius, ASOC split and offset lengths, and the number and relative location of ASOC modules) but differ in suspension and pivot design. This approach was adopted for experimental inspection of the performance of two different designs and tradeoffs between them.

9. MOTOR CONTROL AND COMMUNICATION DESIGN

The requirement that the ASOCs can freely rotate about the axis, α , poses a challenge in terms of cable

layout. There are three potential choices: (1) actuators, a power supply, and computation lie on the central body and power is transmitted mechanically to the wheels; (2) actuators are located on the ASOC, the power supply and computation are located on the central body, and power and control signals are transmitted to the ASOC via slip rings; and (3) each ASOC is a self-contained module comprised of its own power supply, actuators, and local feedback control.

Design (3) was selected since it results in fully modular ASOC units, each capable of performing simple tasks assigned by a supervisory controller. Central computing on the body is required to coordinate the ASOCs and move the vehicle in the proper direction. The schematic layout of the controller structure is presented in Fig. 13.

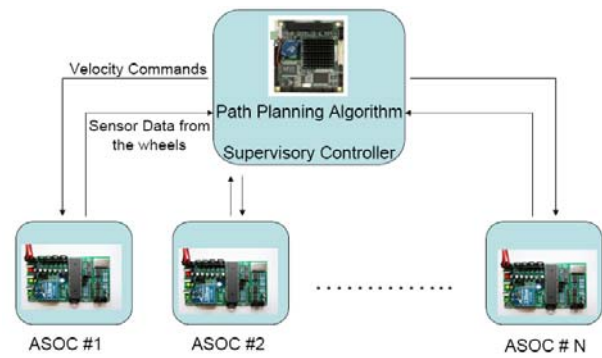


Fig. 13: Control algorithm structure.

There is two-way wireless communication between the ASOC modules and the central control unit. Autonomous operation algorithms and the supervisory control reside in the central unit. The supervisory controller assigns simple tasks for each ASOC in terms of wheel velocity commands. These commands are sent as unicast data frames to each ASOC. Each ASOC in turn performs the following tasks:

- Receive wheel velocity commands from the central unit through wireless communication
- Calculate low-level velocity control for the DC motors
- Condition and collect sensor data
- Provide the central processing unit with the required sensory data to be used by the supervisory controller

10. CONCLUSIONS

In this paper, numerous design considerations were presented for agile, omnidirectional UGVs. An optimization algorithm was implemented to derive values for ASOC module and wheel geometries. The geometric constraints and the optimization algorithm are scalable and can be applied to robots of any size. Two prototype ASOC modules with different suspension designs were

developed. The general operation principle of the UGV controller structure was presented. Future work will include experimental validation of the competing designs.

The development of an omnidirectional UGV for outdoor terrain will provide the US Army with the capabilities to more rapidly and safely complete a number of critical missions now being done by conventional UGVs. The omnidirectional vehicles will be more maneuverable in tight urban quarters and will more easily be able to escape from dangerous situations.

REFERENCES

- [1] Bekker G., 1956: Theory of land locomotion, the mechanics of vehicle mobility, Ann Arbor: The University of Michigan Press.
- [2] Muir, P., and Neuman, C., 1987: Kinematic Modeling for Feedback Control of an Omnidirectional Wheeled Mobile Robot, *Proc. of 1987 IEEE Int. Conf. on Robotics and Automation*, **4**, 1772-1778.
- [3] Park, T., Lee, J., Yi, B., Kim, W., You, B., 2002: Optimal Design and Actuator Sizing of Redundantly Actuated Omni-directional Mobile Robots, *Proc. Of IEEE Intl Conf on Robotics and Automation*, **1**, 732-737.
- [4] Spenko, M., Yu, H., and Dubowsky, S., 2002: Analysis and Design of an Omnidirectional Platform for Operation on Non-Ideal Floors, *Proc of IEEE Intl Conf on Robotics and Automation*, **1**, 726-731.
- [5] Udengaard, M. and Iagnemma, K., 2008: Design of an Omnidirectional Mobile for Rough Terrain, *Proc of IEEE Intl Conf on Robotics and Automation*, 1666-1671.
- [6] Wong J., 1989: Terramechanics and Offroad Vehicles, Amsterdam, Elsevier Science Publishers.
- [7] Yong R, Fattah E, Skiadas N., 1984: Vehicle Traction Mechanics, Amsterdam, Elsevier Science Publishers.
- [8] Yu, H., Dubowsky, S., and Skwersky, A., 2000: Omni-directional Mobility Using Active Split Offset Castors. *Proc of the 26th ASME Biennial Mechanisms and Robotics Conf.*